

Beyond the Standard Model Higgs physics: Hunting $h \rightarrow bs$ with Higgs-strahlung at CEPC and FCC-ee

M. A. Arroyo-Ureña,^{*} Diego Carreño,[†] A. I. García-Gutierrez,[‡] and M. G. Villanueva-Utrilla[§]
*Facultad de Ciencias Físico-Matemáticas, Benemérita Universidad Autónoma de Puebla, C.P. 72570, Puebla, México, and
Centro Interdisciplinario de Investigación y Enseñanza de la Ciencia (CIIEC),
Benemérita Universidad Autónoma de Puebla, C.P. 72570, Puebla, México.*

T.A. Valencia-Pérez[¶]
Instituto de Física, Universidad Nacional Autónoma de México, C.P. 01000, CDMX, México.

The next generation of e^-e^+ colliders, particularly the CEPC and FCC-ee, will offer unprecedented precision to probe Higgs boson properties. In this work, we investigate the flavor-changing decay $h \rightarrow bs$ produced via Higgs-strahlung in the framework of the Two-Higgs-Doublet Model of Type III (2HDM-III). Using multivariate techniques, we project the signal significance for CEPC and FCC-ee, considering dominant backgrounds and systematic uncertainties. Our results demonstrate that these colliders could achieve 5σ sensitivity to $\mathcal{BR}(h \rightarrow bs)$ down to 10^{-4} , providing a unique window into physics beyond the Standard Model.

I. INTRODUCTION

More than twelve years ago, the ATLAS and CMS collaborations announced the observation of a new spin-0 particle with mass $m_h \approx 125$ GeV [1, 2] consistent with the Higgs boson properties predicted by the Standard Model (SM). After its discovery, the Large Hadron Collider (LHC) has characterized the properties of the Higgs boson because, among other things, the Higgs field is fundamental to the generation of the particle masses contained in the SM [3, 4]. As is well known, the SM provides a successful description of the weak, strong, electromagnetic interactions, and many of the experimental observations made in particle physics. Despite these achievements, there are phenomena that cannot be explained within the SM. In particular, Flavor-Changing Neutral Currents (FCNC) Higgs decays in the quark sector are highly suppressed due to the GIM mechanism [5] and the smallness of the Cabibbo-Kobayashi-Maskawa (CKM) quark mixing matrix elements. These decays involve the Higgs boson transforming into a different quark flavor $h \rightarrow q_i q_j$. The theoretical SM predictions of the different channels are given by $\mathcal{BR}(h \rightarrow bs) = 1.78 \times 10^{-7}$, $\mathcal{BR}(h \rightarrow bd) = 8.36 \times 10^{-9}$, $\mathcal{BR}(h \rightarrow sd) = 8.65 \times 10^{-15}$, $\mathcal{BR}(h \rightarrow cu) = 8.13 \times 10^{-19}$ [6]. Since the SM predictions are extremely suppressed, observe them at different rates at colliders like the LHC would be a strong indication of physics beyond the SM. Furthermore, analyze decays like $h \rightarrow q_i q_j$ at proton-proton colliders represent serious challenges, highlighting the large background of QCD which makes it very difficult to identify these kind of processes. In contrast, the next generation of

electron-positron colliders, complementary to the LHC, can study the properties of the Higgs boson -and other particles- with unprecedented precision, high integrated luminosity, high center-of-mass energies, within a very clean background environment. This makes them an excellent option for copiously studying FCNC Higgs decays. Unlike to the Higgs boson production in proton-proton collisions, the environment of e^-e^+ collisions will significantly reduce SM background processes that obscure the signals studied at the LHC or future stages of it, namely, the High-Luminosity LHC [7], High-Energy LHC [8], and the Future hadron-hadron Circular Collider [9]. In this context, the particle physics community has been engaged for many years in the design of several e^-e^+ collider projects: Circular Electron-Positron Collider (CEPC) [10], Future ee Circular Collider (FCC-ee) [11], International Linear Collider (ILC) [12], and the Compact Linear Collider (CLIC) [13]. In this work, we focus on the CEPC and FCC-ee colliders because Higgs boson production is highly favored at a center-of-mass energy of $\sqrt{s} = 240, 350$ GeV. This energy, combined with their projected high integrated luminosity (up to several ab^{-1}) makes CEPC and FCC-ee more advantageous for precision Higgs studies compared to linear colliders like the ILC and CLIC. While the latter can reach higher energies, their integrated luminosities are expected to be significantly lower than those achievable by circular colliders at 240 GeV. The branching ratios for the decays $h \rightarrow bs$ and $h \rightarrow uc$ can be measured at the CEPC with an upper limit $\sim 0.03\%$ and 0.08% at 95% C.L. [14], respectively. A study at the FCC-ee [15] indicates comparable sensitivities of measuring the rates of $h \rightarrow bs$ and $h \rightarrow uc$, estimating the upper limits to be $\mathcal{O}(10^{-3})$. With the possible arrival of these colliders, which have as one of their priorities the study of the Higgs boson, non-standard phenomena could be brought to experimental scrutiny. Due to the advantages of e^-e^+ colliders, FCNC could be of special interest, as they are predicted to have sizeable branching ratios within the theoretical frame-

^{*} marco.arroyo@cfm.buap.mx

[†] diego.carrenod@alumno.buap.mx

[‡] alejandro.garciagut@alumno.buap.mx

[§] maria.villanueva@alumno.buap.mx

[¶] tvalencia@fisica.unam.mx

work of SM extensions. A well-motivated model is the Two-Higgs Doublet Model of type III (2HDM-III), which induces FCNC at tree-level and predicts large rates which can be simultaneously controlled by several mechanisms, such as four-zero textures [16–20], which are invoked in this work.

Thus, we are interested in exploring the prospects of detecting the flavor-changing $h \rightarrow b\bar{s} + \bar{b}s$ decay via the Higgs-strahlung production at CEPC and FCC-ee in the 2HDM-III as it predicts branching ratios for the decay $h \rightarrow bs$ of up to $\mathcal{O}(10^{-5} - 10^{-4})$.

This work is structured as follows. In Sec. II, we describe the relevant aspects of the theoretical framework adopted in this work, *i.e.*, the 2HDM-III with a particular emphasis on the theoretical implications of employing a four-zero texture in the Yukawa Lagrangian. An analysis of the model parameter space is also included. Section III is focused on the study of the proposed signal and its SM background processes. Finally, the conclusions are presented in Sec. IV.

II. TWO-HIGGS DOUBLET MODEL OF TYPE III.

The Two-Higgs Doublet Model includes an additional scalar doublet in contrast to the SM. We denote these doublets as $\Phi_i^T = (\phi_i^+, \phi_i^0)$ ($i = 1, 2$). After Spontaneous Symmetry Breaking (SSB), the Higgs doublets acquire nonzero vacuum expectation values (VEV), given as $\langle \Phi_i \rangle^T = 1/\sqrt{2} (0 \ v_i)$.

The introduction of additional scalar doublet predicts four particles (two neutral and two charged), and gives place to new interactions between the doublets and fermions. The 2HDM-III also leads Flavor-Changing Neutral Interactions (FCNI) at the tree level, which must to be suppressed in order to meet with the experimental observations. In this work, we assume a specific structure of the Yukawa matrices Y_i , the so-called four-zero texture. Using it [20–23], we can effectively control the strength of FCNIs and ensure consistency with the experimental data.

A. Scalar potential

The most general $SU(2)_L \times U(1)_Y$ invariant scalar potential is given by:

$$\begin{aligned} V(\Phi_1, \Phi_2) = & \mu_1^2(\Phi_1^\dagger \Phi_1) + \mu_2^2(\Phi_2^\dagger \Phi_2) - \mu_{12}^2(\Phi_1^\dagger \Phi_2 + h.c.) \\ & + \frac{1}{2}\lambda_1(\Phi_1^\dagger \Phi_1)^2 + \frac{1}{2}\lambda_2(\Phi_2^\dagger \Phi_2)^2 \\ & + \lambda_3(\Phi_1^\dagger \Phi_1)(\Phi_2^\dagger \Phi_2) + \lambda_4(\Phi_1^\dagger \Phi_2)(\Phi_2^\dagger \Phi_1) \\ & + \left[\frac{1}{2}\lambda_5(\Phi_1^\dagger \Phi_2)^2 + \lambda_6(\Phi_1^\dagger \Phi_1)(\Phi_1^\dagger \Phi_2) \right. \\ & \left. + \lambda_7(\Phi_2^\dagger \Phi_2)(\Phi_1^\dagger \Phi_2) + h.c. \right] \end{aligned} \quad (1)$$

We assume that the potential parameters $\lambda_{5,6,7}$ and μ_{12} are reals, even the VEV's. Thus, the CP symmetry is conserved. After the diagonalization of the scalar potential in Eq. (1), the masses of the new particles predicted in the model are given by:

$$\begin{aligned} M_{H^\pm}^2 &= \frac{\mu_{12}^2}{\sin \beta \cos \beta} - \frac{1}{2}v^2(\lambda_4 + \lambda_5 + \cot \beta \lambda_6 + \tan \beta \lambda_7) \\ M_A^2 &= M_{H^\pm}^2 + \frac{1}{2}v^2(\lambda_4 - \lambda_5), \\ M_{H,h}^2 &= \frac{1}{2}(m_{11} + m_{22} \pm \sqrt{(m_{11} - m_{22})^2 + 4m_{12}^2}), \end{aligned} \quad (2)$$

where m_{ij} corresponds to the elements of the real part of the mass matrix \mathbf{M} ,

$$\text{Re}(\mathbf{M}) = \begin{pmatrix} m_{11} & m_{12} \\ m_{12} & m_{22} \end{pmatrix},$$

and are given by

$$\begin{aligned} m_{11} &= v^2(\lambda_1 \cos^2 \beta + \lambda_5 \sin^2 \beta) + \sin^2 \beta m_A^2, \\ m_{12} &= v^2(\lambda_3 + \lambda_4) \cos \beta \sin \beta - \cos \beta \sin \beta m_A^2, \\ m_{22} &= v^2(\lambda_2 \sin^2 \beta + \lambda_5 \cos^2 \beta) + \cos^2 \beta m_A^2. \end{aligned} \quad (3)$$

The angle β defines the ratio of the VEVs such as $\tan \beta = v_2/v_1$ and it mixes the imaginary part with the charged component of Φ_i as follows:

$$\begin{aligned} G_W^\pm &= \phi_1^\pm \cos \beta + \phi_2^\pm \sin \beta, \\ H^\pm &= -\phi_1^\pm \sin \beta + \phi_2^\pm \cos \beta, \\ G_Z &= \text{Im}(\phi_1^0) \cos \beta + \text{Im}(\phi_2^0) \sin \beta, \\ A &= -\text{Im}(\phi_1^0) \sin \beta + \text{Im}(\phi_2^0) \cos \beta, \end{aligned} \quad (4)$$

from which we obtain the charged scalar bosons H^\pm , the pseudo-Goldstone boson associated with the W gauge fields, a CP-odd state A , and the pseudo-Goldstone boson related to the Z gauge boson. Meanwhile, the real part of the scalar doublets Φ_i define two CP-even states through the mixing angle α :

$$\begin{aligned} H &= \text{Re}(\phi_1^0) \cos \alpha + \text{Re}(\phi_2^0) \sin \alpha, \\ h &= \text{Re}(\phi_1^0) \sin \alpha + \text{Re}(\phi_2^0) \cos \alpha, \end{aligned} \quad (5)$$

where

$$\tan 2\alpha = \frac{2m_{12}}{m_{11} - m_{22}}.$$

Eq. (5) gives rise to the SM-like Higgs boson and a CP-even scalar H .

B. Yukawa Lagrangian

The Yukawa Lagrangian of the 2HDM-III reads [24]:

$$\begin{aligned} \mathcal{L}_Y = & - \left(Y_1^u \bar{Q}_L \tilde{\Phi}_1 u_R + Y_2^u \bar{Q}_L \tilde{\Phi}_2 u_R \right. \\ & + Y_1^d \bar{Q}_L \Phi_1 d_R + Y_2^d \bar{Q}_L \Phi_2 d_R \\ & \left. + Y_1^\ell \bar{L}_L \tilde{\Phi}_1 l_R + Y_2^\ell \bar{L}_L \tilde{\Phi}_2 l_R \right), \end{aligned} \quad (6)$$

where $\tilde{\Phi}_j = i\sigma_2 \Phi_j^*$ ($j = 1, 2$). After the SSB, the fermion mass matrices can be defined as:

$$M_f = \frac{1}{\sqrt{2}} \left(v_1 Y_1^f + v_2 Y_2^f \right), \quad f = u, d, \ell. \quad (7)$$

We assume both Yukawa matrices have a four-zero texture form and that are Hermitian [16–20], and are given by

$$Y_1^f = \begin{pmatrix} 0 & d_1^f & 0 \\ d_1^f & c_1^f & b_1^f \\ 0 & b_1^f & a_1^f \end{pmatrix}, \quad Y_2^f = \begin{pmatrix} 0 & d_2^f & 0 \\ d_2^f & c_2^f & b_2^f \\ 0 & b_2^f & a_2^f \end{pmatrix}.$$

The sum of the Yukawa matrices inherits its form to the mass matrix as follows

$$M_f = \begin{pmatrix} 0 & D_f & 0 \\ D_f & C_f & B_f \\ 0 & B_f & A_f \end{pmatrix}. \quad (8)$$

The elements of the fermion mass matrices in Eq. (8) are related to the physical fermion masses m_{f_i} ($i = 1, 2, 3$), via the following invariants:

$$\begin{aligned} \text{Tr}(M_f) &= C_f + A_f = m_{f_1} + m_{f_2} + m_{f_3}, \\ \lambda(M_f) &= C_f A_f - D_f^2 - B_f \\ &= m_{f_1} m_{f_2} + m_{f_1} m_{f_3} + m_{f_2} m_{f_3}, \\ \det(M_f) &= -D_f^2 A_f = m_{f_1} m_{f_2} m_{f_3}. \end{aligned} \quad (9)$$

From Eq. (9), we obtain the relation between the mass matrix elements in its four-zero texture structure and the fermion masses as follows:

$$\begin{aligned} A_f &= m_{f_3} - m_{f_2}, \\ B_f &= m_{f_3} \sqrt{\frac{r_2(r_2 + r_1 - 1)(r_2 + r_2 - 1)}{1 - r_2}}, \\ C_f &= m_{f_3}(r_2 + r_1 + r_2), \\ D_f &= \sqrt{\frac{m_{f_1} m_{f_2}}{1 - r_2}}, \end{aligned} \quad (10)$$

where $r_i = m_{f_i}/m_{f_3}$. Applying a bi-unitary transformation, the fermion mass matrices are diagonalized. However, the Yukawa matrices generally remain non-

diagonal:

$$\bar{M}_f = V_{fL}^\dagger M_f V_{fR} = \frac{1}{\sqrt{2}} \left(v_1 \tilde{Y}_1^f + v_2 \tilde{Y}_2^f \right), \quad (11)$$

where $\bar{M}_f = \text{diag}(m_{f_1}, m_{f_2}, m_{f_3})$ and $\tilde{Y}_a^f = V_{fL}^\dagger Y_a^f V_{fR}$. As a consequence, flavor-changing neutral currents will be induced at tree-level. The fact that M_f is assumed as Hermitian, implies that $V_{fL} = V_{fR} \equiv V_f$. Here, $V_f = \mathcal{O}_f P_f$, where $P_f = \text{diag}\{e^{i\alpha_f}, e^{i\beta_f}, 1\}$ and the \mathcal{O}_f matrix given in Appx. A.

A fact of utmost importance is that $V_{u,d}$ must reproduce the measured matrix elements V_{CKM} , which can be obtained through $V_{\text{CKM}} = V_u^\dagger V_d$, as shown in Ref. [20]. From Eq. (11), we obtain the following expression.

$$\left[\tilde{Y}_a^f \right]_{ij} = \frac{\sqrt{2}}{v_a} \delta_{ij} \bar{M}_{ij}^f - \frac{v_b}{v_a} \left[\tilde{Y}_b^f \right]_{ij}, \quad (12)$$

where

$$\left[\tilde{Y}_b^f \right]_{ij} = \frac{\sqrt{m_i m_j}}{v} \left[\tilde{\chi}_b^f \right]_{ij}, \quad (13)$$

f represent the flavor of fermions, while $\left[\tilde{\chi}_b^f \right]_{ij}$'s are unknown dimensionless parameters. It is important to note that from Eq. (12) different kind of interactions can be defined [24]. In this paper, we select the following definitions

$$\begin{aligned} \left[\tilde{Y}_1^d \right]_{ij} &= \frac{\sqrt{2}}{v \cos \beta} \delta_{ij} \bar{M}_{ij}^d - \tan \beta \left[\tilde{Y}_2^d \right]_{ij} \\ \left[\tilde{Y}_2^u \right]_{ij} &= \frac{\sqrt{2}}{v \sin \beta} \delta_{ij} \bar{M}_{ij}^u - \cot \beta \left[\tilde{Y}_1^u \right]_{ij} \\ \left[\tilde{Y}_1^\ell \right]_{ij} &= \left[\tilde{Y}_1^d \right]_{ij} \quad (d \rightarrow \ell). \end{aligned} \quad (14)$$

From Eqs. (6)-(14), we obtain the $\phi \bar{f}_i f_j$ interactions:

$$\mathcal{L}_Y^\phi = \phi \bar{f}_i (S_{ij}^\phi + i P_{ij}^\phi \gamma^5) f_j, \quad (15)$$

where $\phi = h, H, A$ and

$$\begin{aligned} S_{ij}^\phi &= \frac{g m_f}{2 M_W} c_f^\phi \delta_{ij} + d_f^\phi \left[\tilde{Y}_b^f \right]_{ij}, \\ P_{ij}^\phi &= \frac{g m_f}{2 M_W} e_f^\phi \delta_{ij} + g_f^\phi \left[\tilde{Y}_b^f \right]_{ij}. \end{aligned} \quad (16)$$

In the theoretical framework of the SM, the factors take the values $c_f^{\phi=h} = 1$ and $d_f^{\phi=h} = e_f^{\phi=h} = g_f^{\phi=h} = 0$. Meanwhile, for the 2HDM-III, these coefficients are presented in Table I.

Coefficient	c_f^h	c_f^A	c_f^H	d_f^h	d_f^A	d_f^H
d -type	$-\frac{\sin \alpha}{\cos \beta}$	$-\tan \beta$	$\frac{\cos \alpha}{\sin \beta}$	$\frac{\cos(\alpha-\beta)}{\cos \beta}$	$\csc \beta$	$\frac{\sin(\alpha-\beta)}{\cos \beta}$
u -type	$\frac{\cos \alpha}{\sin \beta}$	$-\cot \beta$	$\frac{\sin \alpha}{\sin \beta}$	$-\frac{\cos(\alpha-\beta)}{\sin \beta}$	$\sec \beta$	$\frac{\sin(\alpha-\beta)}{\sin \beta}$
leptons ℓ	$-\frac{\sin \alpha}{\cos \beta}$	$-\tan \beta$	$\frac{\cos \alpha}{\sin \beta}$	$\frac{\cos(\alpha-\beta)}{\cos \beta}$	$\csc \beta$	$\frac{\sin(\alpha-\beta)}{\cos \beta}$

TABLE I: Coefficients for ϕ -Fermion couplings in 2HDM-III with CP -conserving Higgs potential.

C. Constraints on the 2HDM-III parameter space

A comprehensive analysis on the model parameter space is reported by one of us in Ref. [25], including LHC Higgs boson data [26, 27] through so-called signals strengths. For a decay $S \rightarrow X$ or a production process $\sigma(pp \rightarrow S)$, the signal strength is parameterized as

$$\mu_X = \frac{\sigma(pp \rightarrow h) \cdot \mathcal{BR}(h \rightarrow X)}{\sigma(pp \rightarrow h^{\text{SM}}) \cdot \mathcal{BR}(h^{\text{SM}} \rightarrow X)}, \quad (17)$$

where $\sigma(pp \rightarrow S)$ is the production cross-section of S , with $S = h, h^{\text{SM}}$; here h is the SM-like Higgs boson coming from an extension of the SM and h^{SM} is the SM Higgs boson; $\mathcal{BR}(S \rightarrow X)$ is the branching ratio of the decay $S \rightarrow X$, with $X = c\bar{c}, b\bar{b}, \tau^-\tau^+, \mu^-\mu^+, WW^*, ZZ^*, \gamma\gamma$.

We also confronted the free model parameters against upper limits on the branching ratio of lepton flavor-violating (LFV) processes, $\ell_i \rightarrow \ell_j \gamma$ and $\ell_i \rightarrow \ell_j \ell_k \bar{\ell}_k$ [28], and the decay $B_s^0 \rightarrow \mu^+ \mu^-$ [29], $B_d^0 \rightarrow \mu^+ \mu^-$ [29]¹. These results are directly applicable to our work since most of the parameters that have a direct impact on our predictions were reported, namely:

1. Cosine of the mixing angles: $\cos(\alpha - \beta)$,
2. Ratio of the VEV's: $\tan \beta$,

The parameter space in the $\cos(\alpha - \beta) - \tan \beta$ plane is presented in Fig. 1. The colored points represent these allowed by LHC Higgs boson data (purple points) and upper limits on branching ratios of the lepton flavor-violating processes aforementioned (pink points). The only parameter that was not reported is χ_{bs} , which has its relevance in the FCNI decay $h \rightarrow bs$ through the coupling g_{hbs} , given by

$$g_{hbs} = \frac{\cos(\alpha - \beta) \tan \beta}{\sqrt{2} \sin \beta} \frac{\sqrt{m_s m_b}}{v} \chi_{bs}, \quad (18)$$

To constraint it, we use experimental measurements on $\mathcal{BR}(B_s \rightarrow \mu^- \mu^+)$ [29]. Figure 2 shows the $\chi_{bs} - \tan \beta$ plane, where the red and green points are these allowed

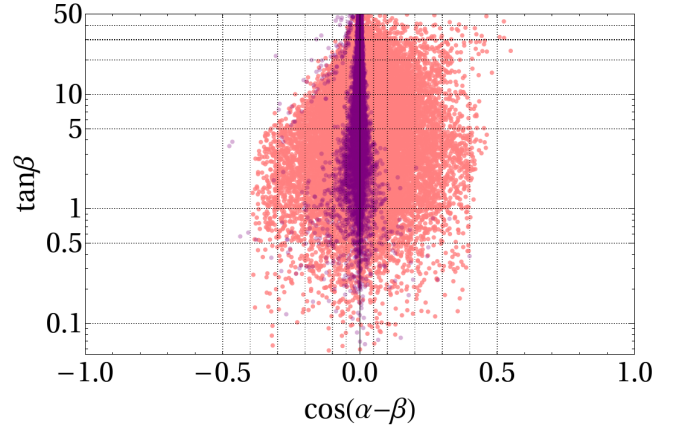


FIG. 1: Allowed parameter space in the $\cos(\alpha - \beta) - \tan \beta$ plane. Pink (Purple) points stand for these allowed values by LHC Higgs boson data (LFV processes). Figure taken from Ref. [25]

by $\mathcal{BR}(B_s \rightarrow \mu^- \mu^+)$ and correspond to $\cos(\alpha - \beta) = -0.05$ and $\cos(\alpha - \beta) = -0.1$, respectively.

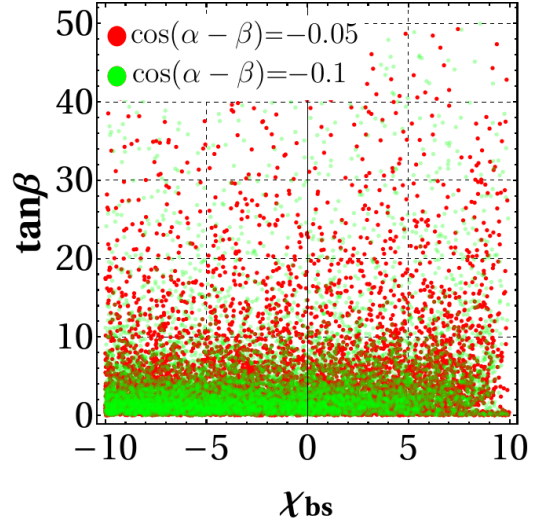


FIG. 2: Allowed parameter space in the $\chi_{bs} - \tan \beta$ plane. Red ($\cos(\alpha - \beta) = -0.05$) and green ($\cos(\alpha - \beta) = -0.1$) points stand for these allowed values by experimental measurements on $\mathcal{BR}(B_s \rightarrow \mu^- \mu^+)$.

From Eq. (18), it is evident that the coupling g_{hbs} is enhanced for large values of $\tan \beta$ and χ_{bs} . Although the constraint from $\mathcal{BR}(B_s \rightarrow \mu^- \mu^+)$ permits sizable values of $\tan \beta$ and χ_{bs} (as illustrated in Fig. 2), we adopt a conservative approach in selecting these parameters to remain within well-motivated theoretical and phenomenological bounds. Thus, we define three Benchmark Points (BMP) to perform realistic predictions in the next section, namely:

- BMP1: $\chi_{bs} = 10, \cos(\alpha - \beta) = -0.1, \tan \beta = 20$,

¹ Analytical expressions for all the LFV processes and the decay $\mathcal{BR}(B_s \rightarrow \mu^- \mu^+)$ in the framework of 2HDM-III also are included in our work [25].

- BMP2: $\chi_{bs} = 10$, $\cos(\alpha - \beta) = -0.05$, $\tan \beta = 10$,
- BMP3: $\chi_{bs} = 5$, $\cos(\alpha - \beta) = -0.05$, $\tan \beta = 10$.

III. COLLIDER ANALYSIS

In this section, we use a Monte Carlo generator to obtain a sample of simulated events with which we explore the prospects for detecting the proposed signal as well as the SM background processes that obscure it. In order to separate the signal from the background, we use the *Boosted Decision Trees* (BDT) machine learning algorithm [30, 31] instead of making direct kinematic cuts as is commonly done. This choice is based on the analysis carried out through the traditional strategy of making hard cuts on the observables, which removes a significant number of background events, but also rejects an important number of signal events. The improvement of BDT compared to “straight” cuts is given by a factor of ~ 6 .

A. Signal and background

- *Signal*: We search in the final state a pair of jets (one of them tagged as a b -jet) and a pair of charged leptons ($\ell^- \ell^+$), which are product of the decays $h \rightarrow bs$ ($bs = b\bar{s} + \bar{b}s$) and $Z \rightarrow \ell^- \ell^+$ ($\ell = e, \mu$), respectively. The Feynman diagram of the signal is presented in Fig. 3

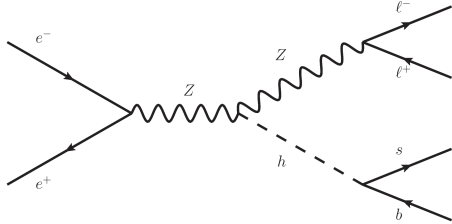


FIG. 3: Feynman diagram of the signal.

We observe from Fig. 3 that the only non standard interaction is hbs , which is given by the following coupling:

$$g_{hbs} = \frac{\cos(\alpha - \beta) \tan \beta}{\sqrt{2} \sin \beta} \frac{\sqrt{m_s m_b}}{v} \chi_{bs}, \quad (19)$$

which makes it evident that the signal increases for high values of $\tan \beta$ and χ_{bs} . The production cross sections of the signal as a function of the center-of-mass energy for the three BMPs are presented in Fig. 4. The vertical lines correspond to different center-of-mass energies associated to the $e^- e^+$ colliders studied in this paper, namely, FCC-ee(H), CEPC, and ILC. The letter (H) of the former indicates its step ($\sqrt{s} = 240$ GeV) in which the Higgs boson will be produced in association with a

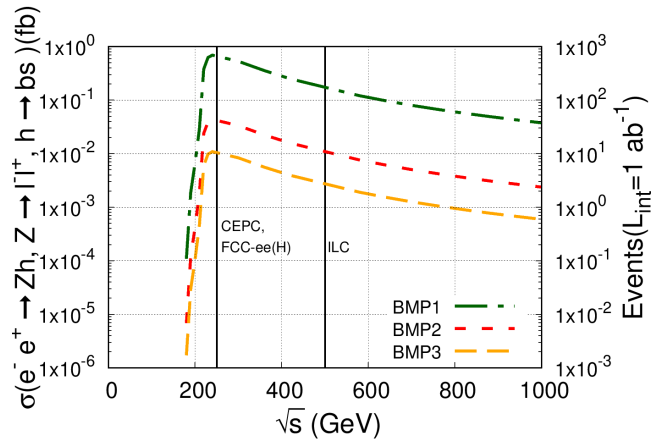


FIG. 4: Cross section of the signal as a function of the center-of-mass energy \sqrt{s} . Vertical lines represent to the energies associated to the different $e^- e^+$ colliders

Z gauge boson. For CEPC and ILC, the vertical lines represent their maximum operating center-of-mass energies. The corresponding integrated luminosities for the aforementioned characteristics are 5600 , 5000 fb^{-1} for CEPC [32], FCC-ee [11], respectively.

- *Background*: The SM background comes from:

$$\begin{aligned} & - e^- e^+ \rightarrow ZZ \rightarrow \ell^- \ell^+ jj, \\ & - e^- e^+ \rightarrow e^- e^+ Z \rightarrow e^- e^+ jj, \\ & - e^- e^+ \rightarrow t\bar{t} \rightarrow W^+ j W^- j \rightarrow \ell^- \bar{\nu}_\ell j \ell^+ \nu_\ell j, \end{aligned}$$

where $j = u, \bar{u}, d, \bar{d}, c, \bar{c}, s, \bar{s}, b, \bar{b}$. It should be noted that the last background process is relevant only for a center-of-mass energy $\sqrt{s} \geq 2m_{\text{top}}$. For CEPC, the highest center-of-mass energy will be $\sqrt{s} = 240$ GeV, for which the process $e^- e^+ \rightarrow t\bar{t}$ is not relevant. However, for FCC-ee it is. Numerical cross sections of the SM background processes at $\sqrt{s} = 240$ GeV and at $\sqrt{s} = 350$ GeV are given in Tables II and III, respectively.

TABLE II: Cross sections of the dominant SM background.

Cross-section	$\sqrt{s} = 240$ GeV
$\sigma(e^- e^+ \rightarrow ZZ \rightarrow \ell\ell jj)$	106.29 fb
$\sigma(e^- e^+ \rightarrow e^- e^+ Z \rightarrow e^- e^+ jj)$	105.74 fb

TABLE III: Cross sections of the dominant SM background.

Cross-section	$\sqrt{s} = 350$ GeV
$\sigma(e^- e^+ \rightarrow ZZ \rightarrow \ell\ell jj)$	62.6 fb
$\sigma(e^- e^+ \rightarrow e^- e^+ Z \rightarrow e^- e^+ jj)$	94.6 fb
$\sigma(e^- e^+ \rightarrow t\bar{t} \rightarrow \ell\ell jj \nu_\ell \bar{\nu}_\ell)$	5.2 fb

The simulations of the phenomenological processes were performed by using `FeynRules` [33] to build the 2HDM-III and produce the UFO files [34], subsequently we generated parton-level events for both the signal and the SM background processes using `MadGraph5` [35], later we performed shower and hadronization with `Pythia8` [36], and finally the detector response has been emulated using `Delphes 3` [37]. According to the information contained in the `Delphes` cards², the b -tagging efficiency is $\epsilon_b = 0.8$, the probability that a c -jet or any other light jet j is mistagged as a b -jet is 0.1 and 0.001, respectively.

1. Signal significance

We now turn to present the most important results we found: the signal significance, which is defined as $\mathcal{N}_S/\sqrt{\mathcal{N}_S + \mathcal{N}_B + (\kappa \cdot \mathcal{N}_B)^2}$, where \mathcal{N}_S (\mathcal{N}_B) is the number of signal (background) events. We assume a total systematic uncertainty combining contributions from b -tagging efficiency (2%), luminosity calibration (1%), jet energy resolution (1%), and background modeling (3%), and it is given by [10]

$$\kappa = \sqrt{(2\%_{b\text{-tag}})^2 + (1\%_{\text{lumi}})^2 + (1\%_{\text{energy}})^2 + (3\%_{\text{modeling}})^2} \approx 4\%. \quad (20)$$

Center-of-mass energy of 240 GeV

Figures 5 and 6 show the signal significance as a function of the integrated luminosity, along with the BDT prediction (using the XGB variable), for the CEPC and FCC-ee(H) at a center-of-mass energy of 240 GeV. According to our analysis, BMP1 emerges as the most promising scenario, exhibiting signal significances of $\geq 5\sigma$ for low integrated luminosities in the ranges of 80–250 fb^{-1} for CEPC and 60–250 fb^{-1} for FCC-ee(H). BMP2 also shows considerable promise, with 3σ evidence and a potential 5σ discovery for integrated luminosities of approximately 1500–5600 fb^{-1} and 4200–5600 fb^{-1} , respectively. In contrast, BMP3 is the least favored scenario, as no significant evidence of the signal is observed.

The XGB variable values fall within the interval 0.5 – 0.99, motivated by the signal and background discriminant shown in Fig. 7 (for the specific case of CEPC and BMP1)³.

To assess the goodness of fit, we applied the Kolmogorov Smirnov (KS) test. The resulting KS values lie within the acceptable range [0, 1], with 0.12 for the

² We use the default `Delphes` cards for CEPC and FCC-ee, `delphes_card.CEPC.tc1` and `delphes_card.IDEA.tc1`, respectively.

³ The remaining classifiers can be generated using the databases from our analysis, which are available upon request.

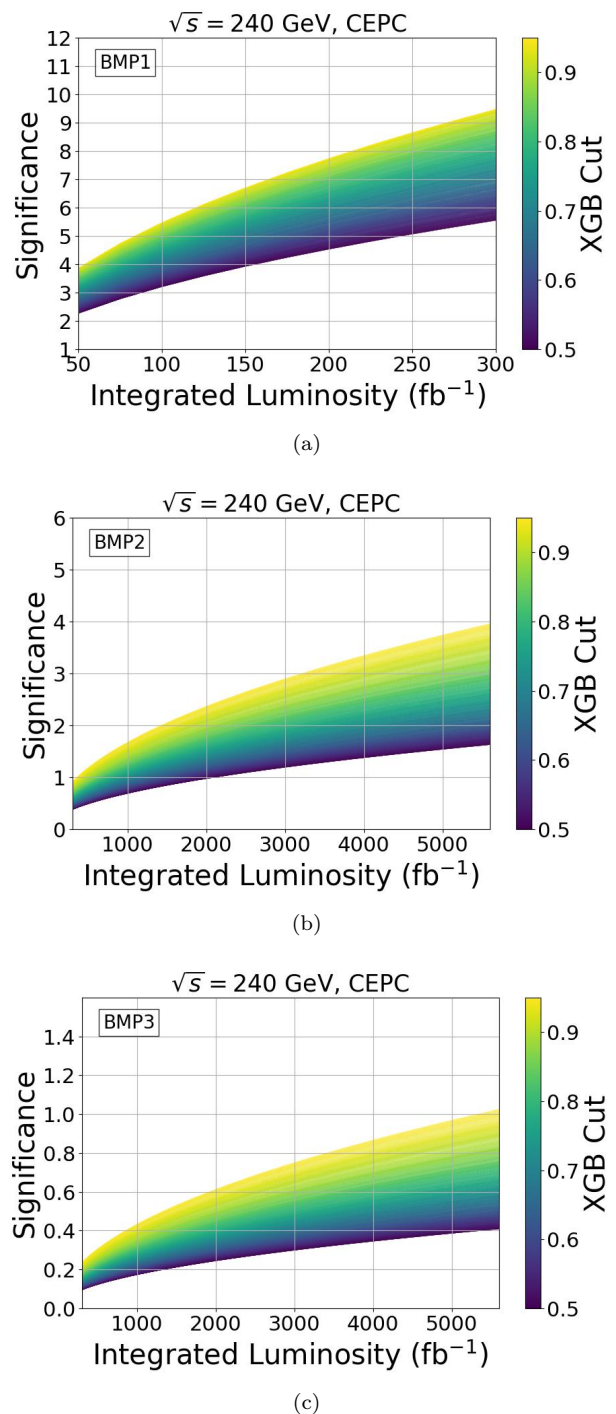
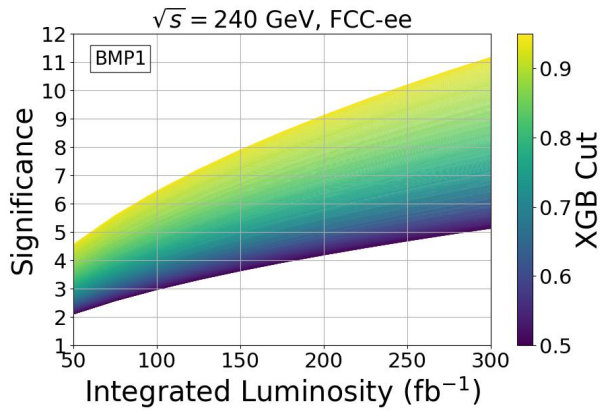
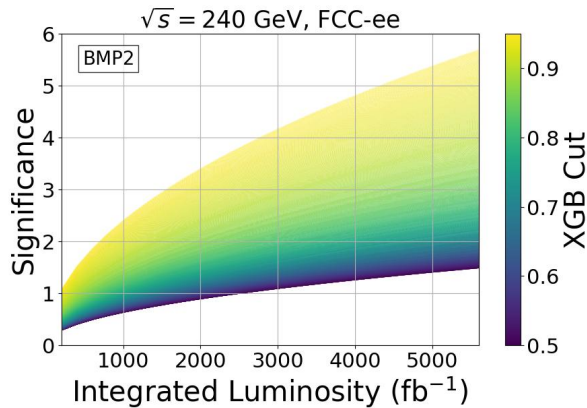


FIG. 5: Signal significance as a function of the integrated luminosity and the BDT variable XGB. This results correspond to a center-of-mass energy of 240 GeV for CEPC, (a) BMP1, (b) BMP2, and (c) BMP3. Systematic uncertainties (4%) are included in the significance calculation via Gaussian smearing of efficiencies.

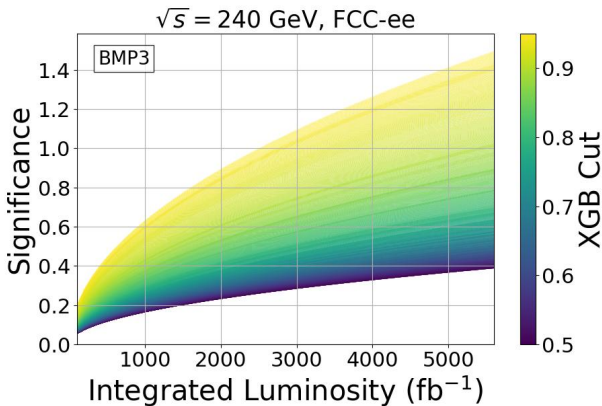
signal and 0.24 for the background. These results con-



(a)



(b)



(c)

FIG. 6: Signal significance as a function of the integrated luminosity and the BDT variable XGB. This results correspond to a center-of-mass energy of 240 GeV for FCC-ee(H), (a) BMP1, (b) BMP2, and (c) BMP3. Systematic uncertainties (4%) are included in the significance calculation via Gaussian smearing of efficiencies.

firm that the training process does not exhibit signs of

overtraining.

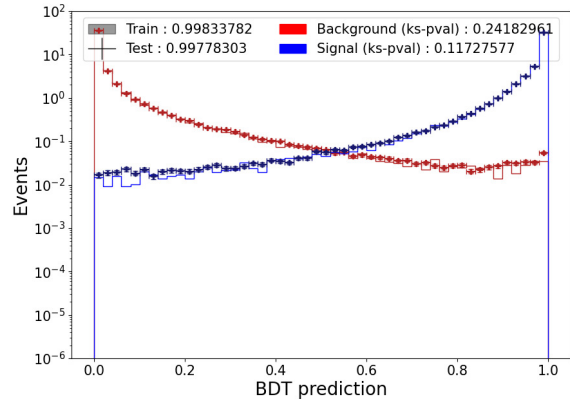
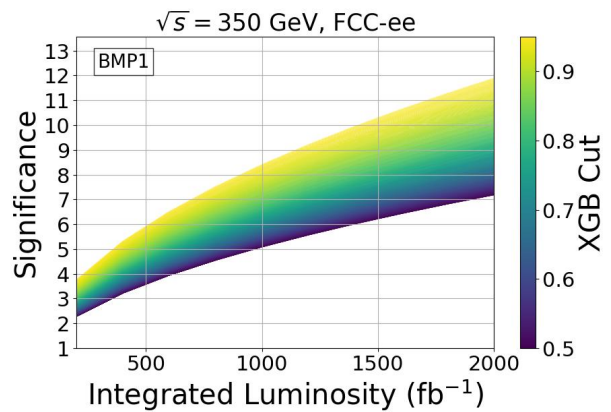


FIG. 7: Plot of the discriminant for signal and background data. This plot corresponds to the CEPC at 240 GeV for BMP1.

Center-of-mass energy of 350 GeV

In contrast to the case at the center-of-mass energy of 240 GeV, the cross section of the signal evaluated at 350 GeV is smaller by a factor of approximately 0.5. In addition, a new background process ($e^-e^+ \rightarrow t\bar{t}$) opens up, which has a significant impact on the signal significance. Similar to the previous scenario at 240 GeV, the most promising result corresponds to BMP1. For this reason, we only present the results for this case in Fig. 8.



(a)

FIG. 8: Signal significance as a function of the integrated luminosity and the BDT variable XGB. This results correspond to a center-of-mass energy of 350 GeV for FCC-ee(H) and BMP1. Systematic uncertainties (4%) are included in the significance calculation via Gaussian smearing of efficiencies.

From Fig. 8 we observe a potential discovery of the signal process if one considers integrated luminosities $\gtrsim 250 \text{ fb}^{-1}$ for FCC-ee. These results, combined with those reported for the 240 GeV case, present an excellent opportunity for experimental scrutiny. Such validation could lead to an irrefutable discovery of physics beyond the SM.

IV. CONCLUSIONS

The search for physics beyond the SM is a key point at the next generation of future e^-e^+ colliders, such as CEPC and FCC-ee. Of particular interest are the flavor-violating processes, as they are very suppressed in the SM. In this work, we have analyzed the flavor-violating process $h \rightarrow bs$ ($bs = b\bar{s} + \bar{b}s$) in the theoretical framework of the 2HDM-III, which predicts for this type of interactions at tree-level, significantly increasing the decay rate. We first have presented the relevant aspects of the 2HDM-III in which our predictions are based. Once we established the theoretical framework, we analyze the prospects for detecting a single Higgs boson in association with a Z gauge boson via the Higgs-strahlung mechanism at e^-e^+ collisions. We searched for the final state $\ell\ell bs$ (where $\ell = e^-, e^+$ or $\mu^-\mu^+$), whose source are the decays $Z \rightarrow \ell\ell$ and $h \rightarrow bs$. To provide realistic predictions, we confront the free parameters of the model against the most up-to-date experimental data, namely, LHC Higgs boson data and upper limits on relevant lepton flavor violation processes. Taking advantage of the insights gained from previous results, we define three benchmark points and we performed a Multivariate Analysis using BDT. We found that the BMP1: $\chi_{bs} = 10$ (parameter responsible for the FCNI $h \rightarrow bs$), $\cos(\alpha - \beta) = -0.1$ and

$\tan\beta = 20$, is the most promising scenario, which is expected since the hbs interaction is favored for large values of $\tan\beta$ and χ_{bs} . Our results allow us to predict for the circular colliders CEPC and FCC-ee at 240 GeV signal significances at level of $\geq 5\sigma$ for integrated luminosities as low as ≈ 80 and $\approx 60 \text{ fb}^{-1}$, respectively. For a center-of-mass energy of 350 GeV, we find similar significance for the FCC-ee. However, larger luminosities are necessary, $\gtrsim 250 \text{ fb}^{-1}$. We encourage experimental collaborations to bring this modest but important contribution to experimental scrutiny, which, if observed, would be compelling evidence of physics beyond the SM.

ACKNOWLEDGMENTS

The work of Marco A. Arroyo-Ureña and T. Valencia-Pérez is supported by “Estancias Posdoctorales por México (SECIHTI)” and “Sistema Nacional de Investigadoras e Investigadores” (SNI-SECIHTI). We thank Haydee Hernández-Arellano for her valuable comments that improved this work and Enrique Díaz for his suggestions on the writing and clarity of the manuscript. T.V.P. acknowledges support from the UNAM project PAPIIT IN111224 and the SECIHTI project CBF2023-2024-548.

Appendix A: Explicit form of the \mathcal{O}_f matrix

The \mathcal{O}_f matrix that diagonalize the fermion mass matrix via $V_f = \mathcal{O}_f P_f$, with $P_f = \text{diag}\{e^{i\alpha_f}, e^{i\beta_f}, 1\}$, is given by

$$\mathcal{O}_f = \begin{pmatrix} \sqrt{\frac{m_{f_2}m_{f_3}(A-m_{f_1})}{A(m_{f_2}-m_{f_1})(m_{f_3}-m_{f_1})}} & \sqrt{\frac{m_{f_1}m_{f_3}(m_{f_2}-A)}{A(m_{f_2}-m_{f_1})(m_{f_3}-m_{f_2})}} & \sqrt{\frac{m_{f_1}m_{f_3}(A-m_{f_3})}{A(m_{f_3}-m_{f_1})(m_{f_3}-m_{f_2})}} \\ -\sqrt{\frac{m_{f_1}(m_{f_1}-A)}{(m_{f_2}-m_{f_1})(m_{f_3}-m_{f_1})}} & \sqrt{\frac{m_{f_2}(A-m_{f_2})}{(m_{f_2}-m_{f_1})(m_{f_3}-m_{f_2})}} & \sqrt{\frac{m_{f_3}(m_{f_2}-A)}{(m_{f_2}-m_{f_1})(m_{f_3}-m_{f_2})}} \\ \sqrt{\frac{m_{f_1}(A-m_{f_2})(A-m_{f_3})}{A(m_{f_2}-m_{f_1})(m_{f_3}-m_{f_1})}} & -\sqrt{\frac{m_{f_2}(A-m_{f_1})(m_{f_3}-A)}{A(m_{f_2}-m_{f_1})(m_{f_3}-m_{f_2})}} & \sqrt{\frac{m_{f_3}(A-m_{f_1})(A-m_{f_2})}{A(m_{f_3}-m_{f_1})(m_{f_3}-m_{f_2})}} \end{pmatrix}, \quad (\text{A1})$$

where m_{f_i} ($i = 1, 2, 3$) are the physical fermion masses

of the three generations.

-
- [1] S. Chatrchyan et al. (CMS), Observation of a New Boson with Mass Near 125 GeV in pp Collisions at $\sqrt{s} = 7$ and 8 TeV, *JHEP* **06**, 081, [arXiv:1303.4571 \[hep-ex\]](#).
 [2] G. Aad et al. (ATLAS), Observation of a new particle in the search for the Standard Model Higgs boson with the ATLAS detector at the LHC, *Phys. Lett. B* **716**, 1

- (2012), [arXiv:1207.7214 \[hep-ex\]](#).
 [3] F. Englert and R. Brout, Broken Symmetry and the Mass of Gauge Vector Mesons, *Phys. Rev. Lett.* **13**, 321 (1964).
 [4] P. W. Higgs, Broken Symmetries and the Masses of Gauge Bosons, *Phys. Rev. Lett.* **13**, 508 (1964).
 [5] L. Maiani, The GIM Mechanism: ori-

- gin, predictions and recent uses, in *48th Rencontres de Moriond on Electroweak Interactions and QCD* (2013) pp. 3–16, [arXiv:1303.6154 \[hep-ph\]](#).
- [6] C. M. Farrera, A. Granados-González, H. Novales-Sánchez, and J. J. Toscano, Quark-flavor-changing Higgs decays from a universal extra dimension, *Int. J. Mod. Phys. A* **35**, 2050141 (2020), [arXiv:2003.05571 \[hep-ph\]](#).
- [7] G. Apollinari, O. Brüning, T. Nakamoto, and L. Rossi, High Luminosity Large Hadron Collider HL-LHC, *CERN Yellow Rep.*, **1** (2015), [arXiv:1705.08830 \[physics.acc-ph\]](#).
- [8] M. Cepeda et al., Report from Working Group 2: Higgs Physics at the HL-LHC and HE-LHC, *CERN Yellow Rep. Monogr.* **7**, 221 (2019), [arXiv:1902.00134 \[hep-ph\]](#).
- [9] N. Arkani-Hamed, T. Han, M. Mangano, and L.-T. Wang, Physics opportunities of a 100 TeV proton-proton collider, *Phys. Rept.* **652**, 1 (2016), [arXiv:1511.06495 \[hep-ph\]](#).
- [10] W. Abdallah et al. (CEPC Study Group), CEPC Technical Design Report: Accelerator, *Radiat. Detect. Technol. Methods* **8**, 1 (2024), [Erratum: *Radiat. Detect. Technol. Methods* **9**, 184–192 (2025)], [arXiv:2312.14363 \[physics.acc-ph\]](#).
- [11] A. Abada et al. (FCC), FCC-ee: The Lepton Collider: Future Circular Collider Conceptual Design Report Volume 2, *Eur. Phys. J. ST* **228**, 261 (2019).
- [12] A. Aryshev et al. (ILC International Development Team), The International Linear Collider: Report to Snowmass 2021, (2022), [arXiv:2203.07622 \[physics.acc-ph\]](#).
- [13] E. Adli et al., The Compact Linear e^+e^- Collider (CLIC), (2025), [arXiv:2503.24168 \[physics.acc-ph\]](#).
- [14] X. Ai et al., Flavor Physics at CEPC: a General Perspective, (2024), [arXiv:2412.19743 \[hep-ex\]](#).
- [15] J. F. Kamenik, A. Korajac, M. Szewc, M. Tammaro, and J. Zupan, Flavor-violating Higgs and Z boson decays at a future circular lepton collider, *Phys. Rev. D* **109**, L011301 (2024), [arXiv:2306.17520 \[hep-ph\]](#).
- [16] H. Fritzsch and Z.-z. Xing, A Symmetry pattern of maximal CP violation and a determination of the unitarity triangle, *Phys. Lett. B* **353**, 114 (1995), [arXiv:hep-ph/9502297](#).
- [17] G. C. Branco, D. Emmanuel-Costa, and R. Gonzalez Felipe, Texture zeros and weak basis transformations, *Phys. Lett. B* **477**, 147 (2000), [arXiv:hep-ph/9911418](#).
- [18] J. Lorenzo Díaz-Cruz, The Higgs profile in the standard model and beyond, *Rev. Mex. Fis.* **65**, 419 (2019), [arXiv:1904.06878 \[hep-ph\]](#).
- [19] J. L. Diaz-Cruz, R. Noriega-Papaqui, and A. Rosado, Mass matrix ansatz and lepton flavor violation in the THDM-III, *Phys. Rev. D* **69**, 095002 (2004), [arXiv:hep-ph/0401194](#).
- [20] M. A. Arroyo-Ureña, J. L. Diaz-Cruz, E. Díaz, and J. A. Orduz-Ducua, Flavor violating Higgs signals in the Texturized Two-Higgs Doublet Model (THDM-Tx), *Chin. Phys. C* **40**, 123103 (2016), [arXiv:1306.2343 \[hep-ph\]](#).
- [21] J. Hernández-Sánchez, C. G. Honorato, S. Moretti, and S. Rosado-Navarro, Charged higgs boson production via cb -fusion at the large hadron collider, *Phys. Rev. D* **102**, 055008 (2020), [arXiv:2003.06263 \[hep-ph\]](#).
- [22] M. A. Arroyo-Ureña, T. A. Valencia-Pérez, R. Gaitán, J. H. Montes De Oca, and A. Fernández-Téllez, Flavor-changing decay $h \rightarrow \tau\mu$ at super hadron colliders, *JHEP* **08**, 170, [arXiv:2002.04120 \[hep-ph\]](#).
- [23] M. A. Arroyo-Ureña, R. Gaitán, E. A. Herrera-Chacón, J. H. Montes de Oca Y., and T. A. Valencia-Pérez, Search for the $t \rightarrow ch$ decay at hadron colliders, *JHEP* **07**, 041, [arXiv:1903.02718 \[hep-ph\]](#).
- [24] J. Hernández-Sánchez, S. Moretti, R. Noriega-Papaqui, and A. Rosado, Off-diagonal terms in yukawa textures of the type-iii 2-higgs doublet model and light charged higgs boson phenomenology, *JHEP* **1307**, 044, [arXiv:1212.6818 \[hep-ph\]](#).
- [25] M. A. Arroyo-Ureña, E. A. Herrera-Chacón, S. Rosado-Navarro, and H. Salazar, Hunting a charged Higgs boson pair in proton-proton collisions, (2024), [arXiv:2405.06036 \[hep-ph\]](#).
- [26] A. M. Sirunyan et al. (CMS), Search for lepton flavour violating decays of the higgs boson to $\mu\tau$ and $e\tau$ in proton-proton collisions at $\sqrt{s} = 13$ tev, *JHEP* **06**, 001, [arXiv:1712.07173 \[hep-ex\]](#).
- [27] G. Aad et al. (ATLAS), Searches for lepton-flavour-violating decays of the higgs boson in $\sqrt{s} = 13$ tev pp collisions with the atlas detector, *Phys. Lett. B* **800**, 135069 (2020), [arXiv:1907.06131 \[hep-ex\]](#).
- [28] R. L. Workman et al. (Particle Data Group), Review of particle physics, *PTEP* **2022**, 083C01 (2022).
- [29] A. Tumasyan et al. (CMS), Measurement of the $B_S^0 \rightarrow \mu^+\mu^-$ decay properties and search for the $B^0 \rightarrow \mu^+\mu^-$ decay in proton-proton collisions at $\sqrt{s} = 13$ TeV, *Phys. Lett. B* **842**, 137955 (2023), [arXiv:2212.10311 \[hep-ex\]](#).
- [30] Y. Coadou, Boosted decision trees [10.1142/9789811234033_0002](#) (2022), [arXiv:2206.09645 \[physics.data-an\]](#).
- [31] T. Hastie, R. Tibshirani, and J. Friedman, *The Elements of Statistical Learning* (Springer, 2009).
- [32] H. Cheng et al. (CEPC Physics Study Group), The Physics potential of the CEPC. Prepared for the US Snowmass Community Planning Exercise (Snowmass 2021), in *Snowmass 2021* (2022) [arXiv:2205.08553 \[hep-ph\]](#).
- [33] A. Alloul, N. D. Christensen, C. Degrande, C. Duhr, and B. Fuks, Feynrules 2.0 - a complete toolbox for tree-level phenomenology, *Comput. Phys. Commun.* **185**, 2250 (2014), [arXiv:1310.1921 \[hep-ph\]](#).
- [34] C. Degrande, C. Duhr, B. Fuks, D. Grellscheid, O. Mattelaer, and T. Reiter, UFO - The Universal FeynRules Output, *Comput. Phys. Commun.* **183**, 1201 (2012), [arXiv:1108.2040 \[hep-ph\]](#).
- [35] J. Alwall, M. Herquet, F. Maltoni, O. Mattelaer, and T. Stelzer, Madgraph 5: going beyond, *JHEP* **06**, 128.
- [36] T. Sjostrand, *PYTHIA 8 Status Report*, Tech. Rep. (DESY, 2009) [arXiv:0809.0303 \[hep-ph\]](#).
- [37] J. de Favereau, C. Delaere, P. Demin, A. Giammanco, V. Lemaitre, A. Mertens, and M. Selvaggi, Delphes 3, a modular framework for fast simulation of a generic collider experiment, *JHEP* **02**, 057.